

Automatic Segmentation of 3D Point Clouds of Rubble Masonry Walls, and its Application to Building Surveying, Repair and Maintenance

Enrique Valero*, Frédéric Bosché, Alan Forster

Institute for Sustainable Building Design, Heriot-Watt University, Edinburgh EH14 4AS, UK

*Corresponding author. e.valero@hw.ac.uk

Abstract – Changing climatic conditions are contributing to faster deterioration of building fabric. Increasing number of heavy rainfall events can particularly affect historic and Cultural Heritage (CH) buildings. These evolving and uncertain circumstances demand more frequent survey of building fabric to ensure satisfactory repair and maintenance. However, traditional fabric surveys have been shown to lack efficiency, accuracy and objectivity, hindering essential repair operations. The recent development of reality capture technologies, together with the development of algorithms to effectively process the acquired data, offers the promise of transformation of surveying methods.

This paper presents an original algorithm for automatic segmentation of individual masonry units and mortar regions in digitised rubble stone constructions, using geometrical and colour data acquired by Terrestrial Laser Scanning (TLS) devices. The algorithm is based on the 2D Continuous Wavelet Transform (CWT), and uniquely it does not require the wall to be (nearly) perfectly flat or plumb. This characteristic is important because historic structures, in particular, commonly present non-negligible levels of bow and waviness and out-of-verticality.

The method is validated through experiments undertaken using data from two relevant and highly significant Scottish CH buildings. The value of such segmentation to building surveying and maintenance regimes is also further demonstrated with application in automated and accurate measurement of mortar recess and pinning. Overall, the results demonstrate the potential of the automatic segmentation of masonry units towards more comprehensive and accurate surveys.

Keywords: point cloud processing, heritage science, masonry, stone, surveying, segmentation, continuous wavelet transform

1. Introduction

One fifth of all buildings in Scotland are characterised as being historic. This includes more than 400,000 buildings that were constructed before 1919 [1]. It is intuitive that the repair and maintenance of these aging structures is becoming increasingly onerous due to degradation processes and the sheer age of the materials employed. Compounding this, it is well recognised that climate change is placing significant performance strain upon the existing built environment, ostensibly due to increased intensity and frequency of rainfall events in the UK [2] [3]. Within the context of a northern maritime climate, these buildings are wetter for longer and are often situated in environments with low potential evaporation [4]. Increased and accelerated deterioration of porous building materials subjected to saturated conditions is correlated with higher incidence of high and low order magnitude spalling associated with frost, increased biological activity, and salt related damage [5] [6] [7] [8].

Aging fabric, twinned with increasingly aggressive environmental conditions, necessitates greater levels of contextualised building survey for effective targeted remedial intervention. Protocols and

45 processes currently employed support conservation activities, ideally creating an objective datum for
46 intervention. Nevertheless, these can be costly to undertake and place significant economic strain
47 upon individuals and organisations entrusted with satisfactory building upkeep. These protocols are
48 principally traditional in nature, adopting visual / manual evaluation of masonry elements, down to
49 individual units. Additionally, inability to effectively record rubble masonry creates communication
50 problems for those developing repair strategies, specifying remedial works or undertaking fabric
51 intervention.

52 Attempts to record via hand drawing is cost prohibitive and is therefore only traditionally undertaken
53 for buildings of the greatest significance or in the case of specialist studies focusing upon
54 archaeological analysis or for academic purposes (see [9]). Furthermore, hand drawing is prone to
55 inaccuracy due to its inherent complexity, resulting from a lack of uniformity, roundness and regularity
56 of masonry units. Given this, a default of generic hatching (labelling) of the material is applied to
57 approximate areas to be highlighted. This is clearly insensitive in capturing and reflecting the reality
58 of the as-built materials confronting the evaluator, hindering attempts to specifically identify areas
59 requiring further assessment. In these situations, recording is therefore practically reduced to
60 narrative description of the masonry wall area (in m^2) and cannot effectively reflect the complexity of
61 the build. Importantly, such recording does not offer the ability to readily locate individual stones in
62 what could be described as a 'sea of stones', causing communication problems for current and future
63 information retrieval.

64 Attempts to enhance reporting uniformity have led to the utilisation of system-based approaches or
65 protocols to survey [10] and whilst helpful, they cannot discount the inherent variation in surveyors'
66 experience [11].

67 The use of state-of-the-art remote sensing technologies offers the promise of enhanced survey
68 accuracy with the logical benefits that flow from primary characteristics such as cost, safety and
69 objectivity. Reflecting this, various researchers have cumulatively progressed the body of knowledge
70 on the value of these new technologies to support building surveying and maintenance activities.

71 In 1995, Ogleby [12] undertook a comprehensive review of techniques and technologies that existed
72 for the generation of information adopted for the historic interpretation of monuments and sites of
73 cultural significance. In that paper, the author focused on photogrammetric applications and the
74 subsequent generation of CAD models. Further geospatial data acquisition technologies, and more
75 specifically Terrestrial Laser Scanner (TLS) and photogrammetry, have revolutionized the recording
76 and documentation aspects of historic buildings. Within the context of historic buildings surveying,
77 Wilson et al. [13] illustrated the benefits of TLS contextualised upon complex UNESCO World Heritage
78 sites, adopting a case study approach. Similar advances have been made using photogrammetry,
79 taking advantage of rapid progress in photographic technology and computer vision. High-resolution
80 cameras are now widely available at a relatively low cost, and the development of robust automated
81 feature detection and matching in digital images, (e.g. SIFT [14] or SURF [15] features), as well as dense
82 matching approaches [16] have considerably improved the image processing stage, enabling entirely
83 automated processing pipelines. More recently, strategic use of Unmanned Aerial Vehicles (UAVs) for
84 reality capture has been providing a new platform for photogrammetry to partially solve access issues.
85 The value of UAVs to surveying has already been demonstrated in various contexts such as for
86 ecological [17] or structural surveys [18]. These works illustrate how to obviate the use of scaffold and
87 are therefore clearly beneficial in reducing acquisition time and cost. In the context of historic
88 monuments, UAV-based photogrammetry has been shown to provide alternative solutions to TLS. For
89 example, Puschel et al. [19] proposed the use of terrestrial and UAV pictures to capture and create an
90 accurate 3D model of Castle Landenberg. Koutsoudis et al. [20] similarly proposed a photogrammetric

91 system combining UAV and terrestrial pictures, and compared the resulting reconstruction with TLS,
92 obtaining promising results.

93 These technologies have proven to be effective, delivering accurate 3D and colour measurements.
94 However, the outcome obtained by the mentioned devices are in raw data form (point clouds) and
95 require further processing to produce understandable semantically-rich information that can be
96 interpreted by experts.

97 With respect to the analysis of geospatial data, initial identification of primary building volumes or
98 entities can be considered as a 1st order structure tier, with 2nd order tiers including subdivisions into
99 principle building components such as walls, roofs, etc. The segmentation of the individual masonry
100 units can be considered as 3rd order structure tier. But, as noted earlier, such segmentation is rarely
101 conducted, let alone systematically successfully achieved, due to the sheer number of stones, the lack
102 of uniformity in the materials, and the subjectivity of the individual surveyors observing the structures.
103 Yet, whilst difficult to achieve, this is an essential component of other tangible processes (i.e. effective
104 costing of the works and the development of repair strategies).

105 Within this context, objective and cost-effective data processing methods are required to facilitate
106 reporting and analysis. Automatic segmentation and further processing of data from modern reality
107 capture technologies (i.e. TLS and photogrammetry) would facilitate surveying operations undertaken
108 by surveying experts, enabling them to focus on value-adding activities such as conducting building
109 pathology from identified defects, and developing in-depth repair strategies. Various research teams
110 have been specially working on advancing this field. Most prominently, a semi-automatic delineation
111 and masonry classification was developed by Oses and Dornaika [21] who used Artificial Intelligence
112 techniques (k-NN classifiers) to identify stone blocks in 2D images. Additionally, Cappellini et al. [22]
113 proposed a semi-automatic approach to semantically label 2.5D data (colour and depth information)
114 of brick and stone walls obtained using photogrammetry.

115 Whilst data segmentation and subsequent calculations, in both visual and computer-based surveys,
116 are relatively easy to achieve in brickwork, squared coursed rubble and ashlar, these calculations are
117 inherently more complex in the case of random rubble masonry due to variability in stone and mortar
118 dimensions. The objective of this paper is to present a novel approach to deal with the segmentation
119 of masonry walls made of irregular rubble or 'random' rubble. The method, detailed in the next
120 sections, is based on the analysis of 2.5D wall data (acquired by means of TLS) in the spatial frequency
121 domain, by means of the 2D Continuous Wavelet Transform (CWT). This mathematical tool, as shown
122 in [23], allows a detailed analysis at local level and is not sensitive to more global levels of flatness,
123 waviness, curvature and plumbness of walls, which are commonly encountered in historic buildings.

124 The rest of the paper is structured as follows: Section 2 contains an introduction to the CWT. Section
125 3 describes the method designed for stone/mortar segmentation. Section 4 presents how such
126 segmentation can effectively further analysis of value to building surveying and maintenance, with the
127 example of mortar regression from the masonry surfaces. Section 5 introduces the experiments
128 carried out to test the developed technique and reports the obtained results. Section 6 concludes the
129 works and offers directions for future works.

130 2. 2D Continuous Wavelet Transform for Stone Walls Segmentation

131 The Wavelet Transform is a signal analysis method that is based on the convolution of the input signal
132 with a wavelet function at different locations along the signal and at multiple scales. This enables the
133 detection of the signal pattern of the wavelet function at potentially any scale and at any location [24].

134 The Continuous Wavelet Transform (CWT) is one of the several variants of the Wavelet Transform that
135 is commonly considered for pattern or frequency detection in a signal. This can be applied to solve the
136 problem of surface waviness characterizations [24]. It is important to highlight that CWT is not only
137 applicable to 1D signals, but also to 2D signals, as presented in [25].

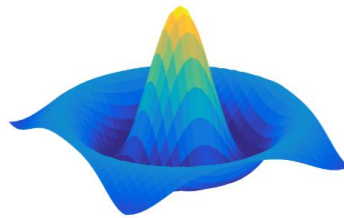
138 Applying the CWT, like any other WT, requires the selection of the mother wavelet. One common CWT
139 wavelet is the Mexican Hat wavelet, as shown in Figure 1. This 2D wavelet is composed of one main
140 undulation with centre frequency f_c that is the same for both dimensions. The centre frequency of the
141 Mexican Hat wavelet is $f_c=0.252$. By convolving an input 2D signal with the Mexican Hat wavelet at a
142 given scale a , undulations of characteristic frequency f can be detected; f is calculated as:

143

$$f = \frac{f_c}{\delta_p a} \quad (1)$$

144 where δ_p is the point sampling period in the input signal along the given dimension.

145



146

147

Figure 1: 3D view of the 2D Mexican Hat wavelet

148

149 In the case of the point cloud of a wall or any other structural surface, the 3D dataset can be
150 transformed into a depth map (i.e. a 2.5D dataset) with cell size δ_p . The 2D CWT can then be applied
151 to the transformed data to detect and precisely locate the stones on the wall. Importantly, the stone
152 walls, constituted of both ashlar and/or random rubble components, may vary in shape and size,
153 especially in the case of walls containing rubble. Therefore, the dimension of the stones cannot be
154 used as a reference scale a for the CWT. However, joints between stones are relatively regular in
155 width. This expected width can be used to set the scale a at which the CWT must be applied so that it
156 responds strongly in mortar regions.

157

158 3. Method for stone segmentation and labelling

159 This section is dedicated to illustrating how the CWT is used to segment individual stones in a 3D point
160 cloud.

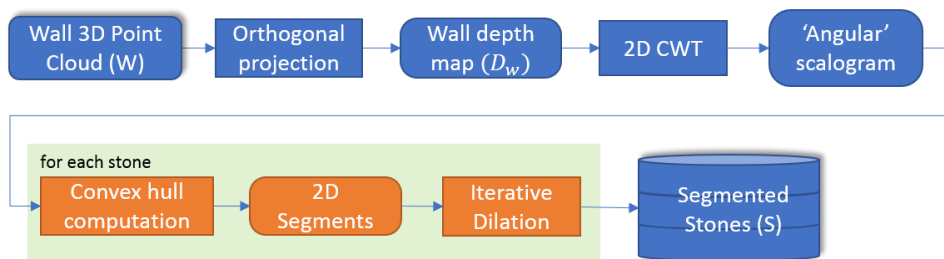
161 Data acquisition and pre-processing of the data, corresponding to the aforementioned 1st and 2nd
162 order structure tier classification (wall segmentation), lead to coloured point clouds of the wall face
163 such as the one depicted in Figure 2. This data is inputted into the segmentation algorithm, which is
164 summarised in Figure 3. The region highlighted in Figure 2 is used as an example to illustrate the
165 segmentation process described below. Figure 4 shows the results obtained for that section of wall at
166 each stage of the process, with Figure 4(a) showing the initial 3D point cloud of that region.



167

168
169

Figure 2: West wall of Linlithgow Palace courtyard. The highlighted area is used in Figure 4 to illustrate the data processing stages.



170

171
172

Figure 3: Overview of the proposed stone segmentation pipeline. The section in the green box includes the operations performed on each individual stone segment and shadow boxes correspond to 3D data

173

174 First, the data is converted into a 2D depth map (also called 2.5D map) by means of an orthogonal
 175 projection on a (vertical) surface grid defined with a regular sampling δ_p . This grid is calculated
 176 following a strategy based on the RANSAC algorithm [26] in the case of walls whose two principal
 177 curvatures are close to zero (i.e. planar walls). If one of these curvature values is not close to zero,
 178 such as with round tower walls, a cylinder is instead calculated as a reference geometry [27]. The value
 179 of each grid depth map pixel is then calculated as the mean distance, to the fitted surface, of the set
 180 of points that fall within it by orthogonal projection. In the case of the use of a cylindrical reference
 181 surface, this is achieved by *unwrapping* the point cloud using the approach described in [28]. An
 182 example of a depth map is shown in Figure 4(b).

183 The 2D CWT is applied to the depth map using an estimate of the mortar joint width to define the
 184 scale of interest a . The CWT process delivers a scalogram, showing the CWT responses at each pixel
 185 in the depth map. Angular values corresponding to scalograms for three different frequencies below
 186 the characteristic frequency f (i.e. defined scale a) are shown in Figure 4(c); the angular values
 187 obtained for the characteristic frequency f are shown in Figure 4(d). With the objective of avoiding
 188 under-segmentation, a conservative strategy is followed when defining the width of mortar joints, i.e.
 189 the scale a . The value of a used in this method is 1.2 times a coarse average width of the mortar joints
 190 estimated by the surveyor.

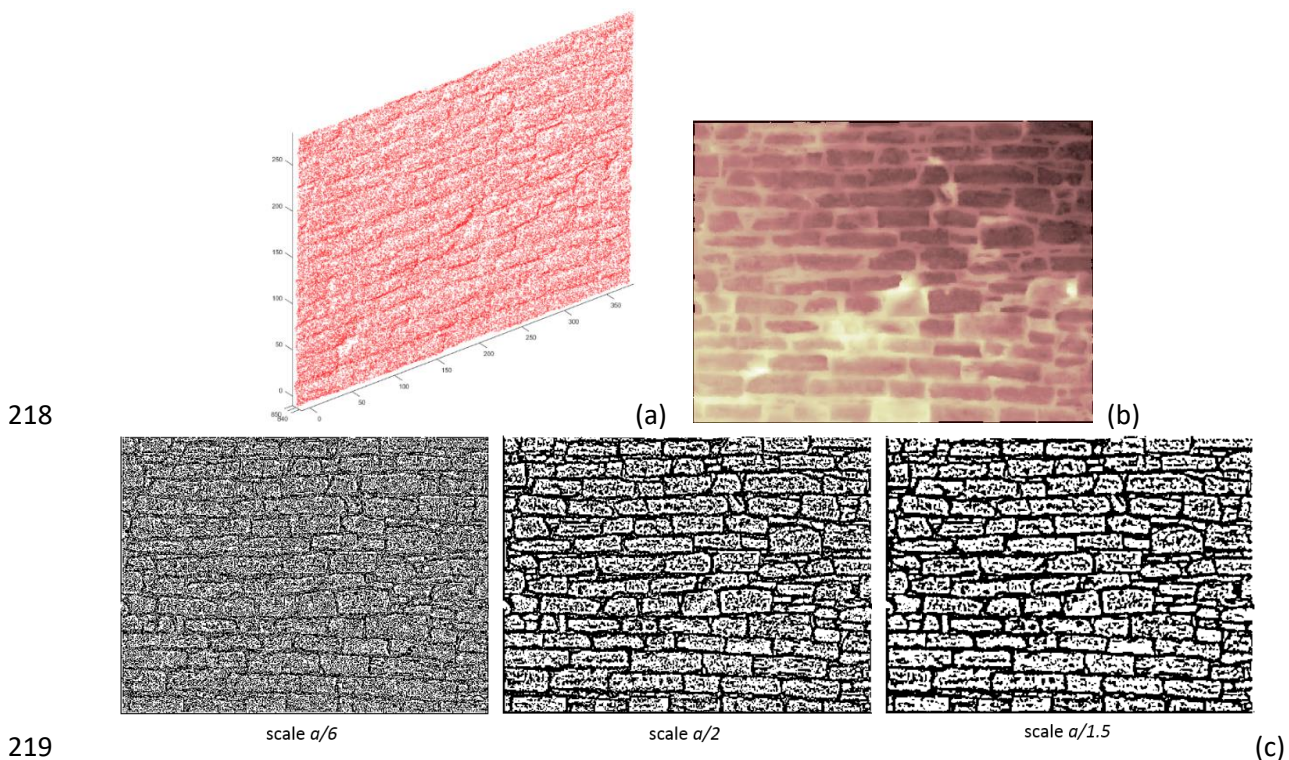
191 Note that, whilst no value is given for the width of a rubble masonry joint due to the variability of the
 192 masonry deployed (See [29]), certain physical characteristics in the associated use of lime mortars
 193 direct us towards a nominal width dimension of approximately 15-20mm [30]. More specifically, the
 194 relative slow set of lime mortars makes it vulnerable to moisture related shrinkage during curing. This
 195 phenomenon is reduced by adopting a 'well graded' aggregate and, in situations where the joint is
 196 wider the utilisation of suitable pinning stones (off cuts or small stones that are pushed or built into

197 the mortar joint) are adopted. It is therefore empirically essential to keep the overall volume of mortar
198 in the joint to a minimum, by packing with suitable pinnings, and to thoroughly compact the mortar.
199 Deviation from this heuristic could result in materials failure. However, it must be noted that such
200 modern practice did not apply in historic rubble masonry wall, and it is common in such contexts that
201 the width of mortar joints be 30-40mm. Therefore, in this work, we ask that the surveyor provides as
202 input an estimate width of mortar joints according to the evaluated façade (which will typically be
203 either 20mm or 40mm).

204 The binary image delivered by the 2D CWT contains an approximated segmentation of the stones.
205 However, as illustrated in Figure 4(d), such irregularities of the surface profile of the rubble stones can
206 generate concavities that lead to strong responses of the CWT (see small black areas inside the white
207 segments in Figure 4(d)). To correct this, we make the observation (and assumption) that rubble
208 stones are normally contained exactly within their convex hull. Thus, we replace each white segment
209 with its convex hull. Figure 4(e) shows the result.

210 As previously mentioned, a slightly higher value for the scale a is used as input for the CWT. While this
211 increases the performance of the segmentation, it also leads to stone segments that are moderately
212 smaller than their actual size (and conversely mortar joints moderately wider than their actual width).
213 To correct this effect, an iterative dilation process (1 pixel per iteration) is performed for each stone
214 segment, considering colour information from the associated point cloud.

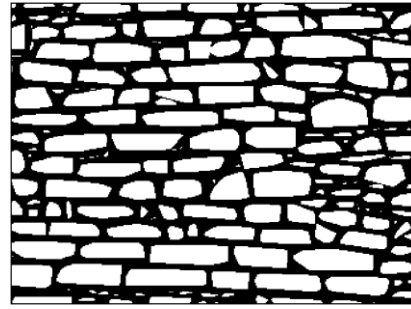
215 At the end of the dilation process, 2D stones segments are considered to be properly defined, as
216 illustrated in Figure 4(f). Figure 4(g) shows the final segmentation results re-mapped on the 3D point
217 cloud.



220



(d)

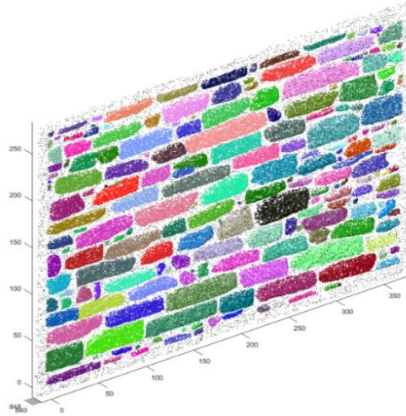


(e)

221



(f)



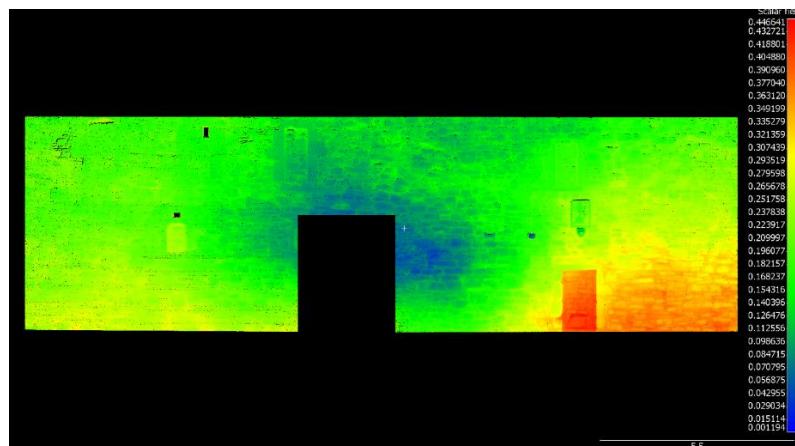
(g)

222 *Figure 4: Illustration of the stone segmentation process. a) Input wall 3D point cloud, b) depth map, c) 2D CWT scalogram*
 223 *for the selected scale a, d) 2D stone segments after convex hull step, e) 2D stone segments after the final dilation step; and*
 224 *f) final segmentation re-mapped onto the 3D point cloud.*

225

226 Importantly, we note that the CWT response is not sensitive to frequencies that are much lower than
 227 the characteristic frequency. This means that variations in the flatness, waviness and curvature of
 228 walls with such low frequency (i.e. large wavelength) do not impact the response of a wavelet used to
 229 detect high frequencies representing mortar joints. Figure 5 illustrates planarity disparities typically
 230 observed in historic masonry walls. This particular wall is used in our validation experiments for which
 231 the results are presented in Section 5.

232



233

234

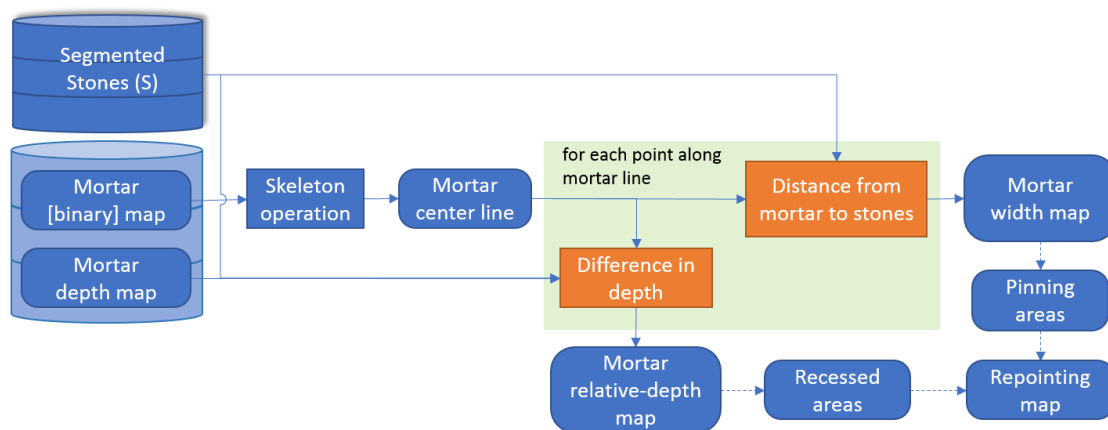
234 *Figure 5: Local depth values in a rampart of Craigmillar Castle (Scotland)*

235

236 4. Application of the stone segmentation through further analysis

237 The segmentation achieved with the described algorithm can be used for the evaluation of materials
238 and their associated construction technologies. Additionally, when utilised in repeated survey
239 operations it can move beyond 'static' determination of condition and enable analysis of progressive
240 defects. More specifically, stone segmentation can be used to evaluate changes in individual stones
241 (e.g. erosion or movement) and record those changes down to individual stone level. Segmented
242 mortar joint regions can be further analysed to deliver valuable information on their conditions and,
243 by extrapolation, the effect of deterioration on surrounding masonry.

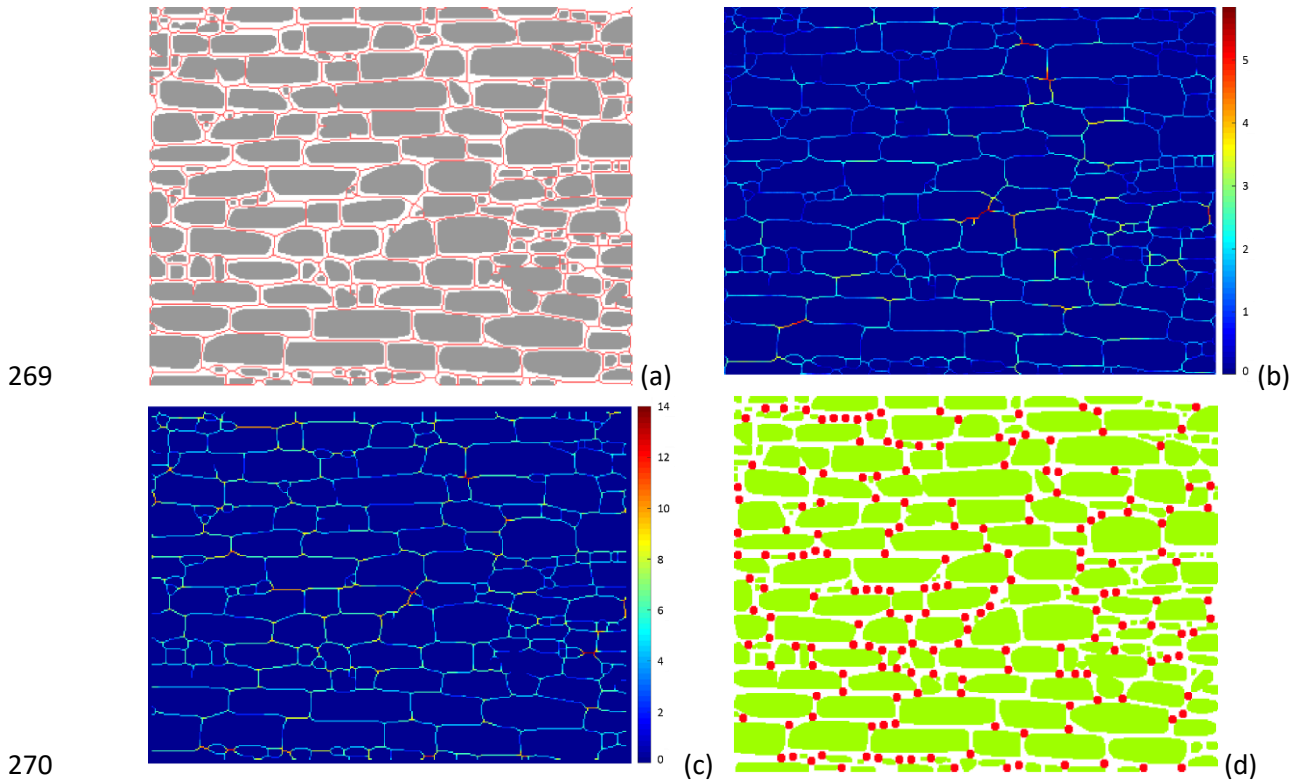
244 To demonstrate this, we present an additional data processing algorithm that analyses the mortar
245 region segments outputted by the previous algorithm to report the mortar region linear measurement
246 and calculate depth profiles along the mortar centre lines. This constitutes important information to
247 detect recessed zones, and accurately estimates the quantity of repointing to be undertaken. In
248 addition, depth of joint recess is a primary mechanism for highlighting vulnerable areas of masonry
249 that may be subject to progressive loosening of the material if left unattended. The system can also
250 automatically estimate the mortar region width, which can inform on the need for pinning (a.k.a.
251 gallets). The following explains the developed algorithm. Figure 6 summarises the approach and Figure
252 7 illustrates each of its steps.



253
254 *Figure 6: Overview of the proposed mortar region analysis pipeline. The objects coloured in orange represent the operations*
255 *performed on each individual stone segment*

256
257 The depth and binary maps for the mortar region(s) obtained from the segmentation process are used
258 as inputs in this process. A skeleton operation [31] is first applied to the binary map to obtain the
259 centre lines of the mortar areas (Figure 7(a)). For each point along the centre line of the mortar
260 regions, its depth value is compared to those of the neighbouring stones, delivering the depth
261 difference between stones and mortar (Figure 7(b)). This mortar relative-depth map can be used to
262 identify recessed regions.

263 In a similar manner, the orthogonal distance between each point along the centre line and the
264 neighbouring stones is calculated to obtain a mortar width map, (Figure 7(c)). The depth and width
265 maps can be employed jointly to calculate the volume of mortar required for repair and determine
266 areas where pinning stones may be required. This is illustrated in Figure 7(d) that has been
267 produced by assuming that pinning is required where mortar width is larger than the scale a used in
268 the 2D CWT).



271 *Figure 7: Maps obtained after processing the data of mortar regions. a) Centre lines of the mortar areas (in red). b) Relative*
 272 *depth of mortar along the centre line (cm). c) Width of mortar along the centre lines (cm). d) Potential pinning stone*
 273 *locations (in red)*

274

275 **5. Experimental results**

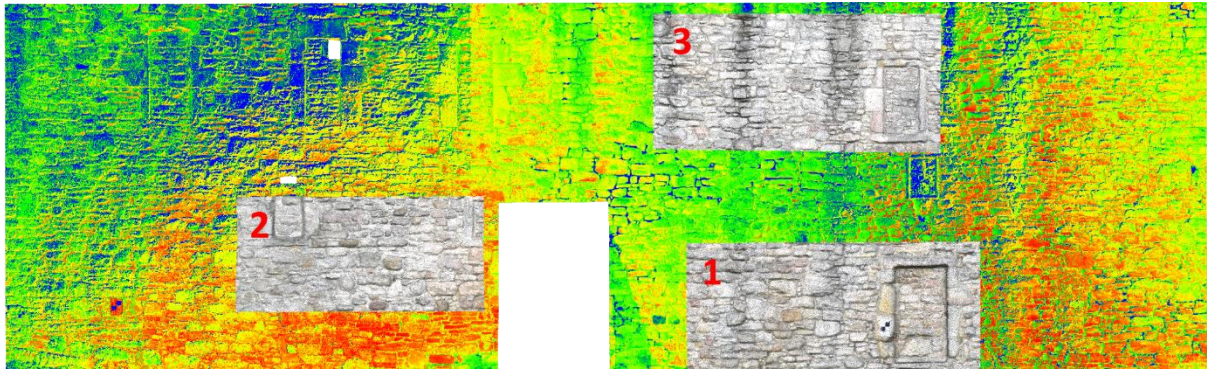
276 The algorithms presented in the previous sections have been tested with dense point clouds acquired
 277 from several walls at two significant Scottish Cultural Heritage buildings, namely: Craigmillar Castle
 278 and Linlithgow Palace. In the case of Craigmillar Castle, a Faro Focus 3D Laser Scanner digitised the
 279 scene, providing 3D and colour information, with a resolution of 3mm. In Linlithgow Palace, a Leica
 280 P40 Terrestrial Laser Scanner was used for data acquisition, delivering colour and geometric
 281 information, with a resolution of 2mm.

282 In this section, two different experiments are presented, at both small and large scale, to illustrate:
 283 first, the accuracy of the proposed system and secondly, the potential of the tool to be used for
 284 maintenance, repair and interpretation works in complete walls (i.e. building elevations).

285 **5.1. Quantitative assessment of the segmentation method**

286 In this subsection, a quantitative evaluation of the method's accuracy is presented. Three rectangular
 287 sections of masonry with approximate area 30m² from a Craigmillar Castle rampart wall were selected
 288 (see highlighted areas in Figure 8). Note the presence of blocked-up windows, with stones laid in
 289 different planes, is challenging.

290 The three regions are at different heights (ground level, 2 and 5 meters) and have been selected for
 291 the diversity of wall conditions they present.



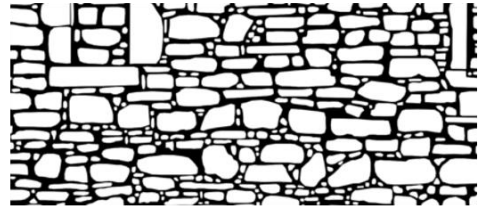
292

293 *Figure 8: Three masonry sections selected for assessing the performance of the proposed algorithm*

294

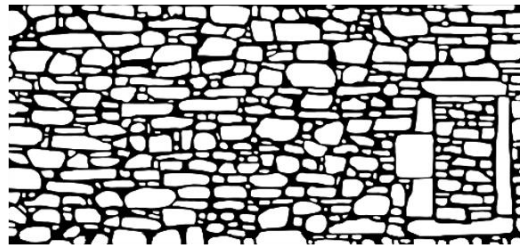
295 First, for each selected region, a manual segmentation of the stones' boundaries is performed on the
296 colour/depth maps. The resulting segmentation maps (see binary maps in Figure 9) are then used as
297 ground truth. The results of the automated segmentation achieved by the proposed algorithm is also
298 shown in Figure 9.

299 The manual segmentation delivers an area covered by the segmented stones of $18.61 m^2$. The
300 proposed algorithm reports that $17.76 m^2$ is covered by the segmented stones. The difference results
301 in an error of 4.6%. With respect to the mortar regions, the algorithm estimates 325.37 m of mortars,
302 whereas the manual segmentation led to 312.06 m, which gives an error of 4.26%.



(a)

(b)



(c)

303

304

305

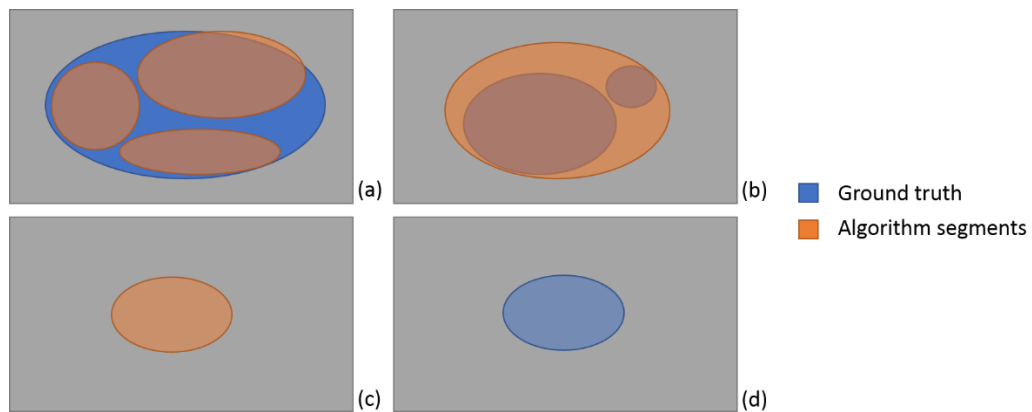
306

307

Figure 9: Wall segmentation results. a) Section 1, b) Section 2 and c) Section 3. For each section, top: 3D point cloud of the wall section; middle: manual segmentation of the orthographic projection of the wall; bottom: orthographic projection of the labelled segments.

308 The difference between manual and automatic segmentations is primarily due to four factors (see
 309 Figure 10):

- 310 a) Under-estimation: some stones are detected as a combination of smaller stones;
- 311 b) Over-estimation: some stones are segmented as a unique stone;
- 312 c) False stone: some mortar areas are labelled as stone; and
- 313 d) Missing stones: some small stones have not been identified.



314
 315 *Figure 10: Issues in the segmentation of stones and mortar*

316

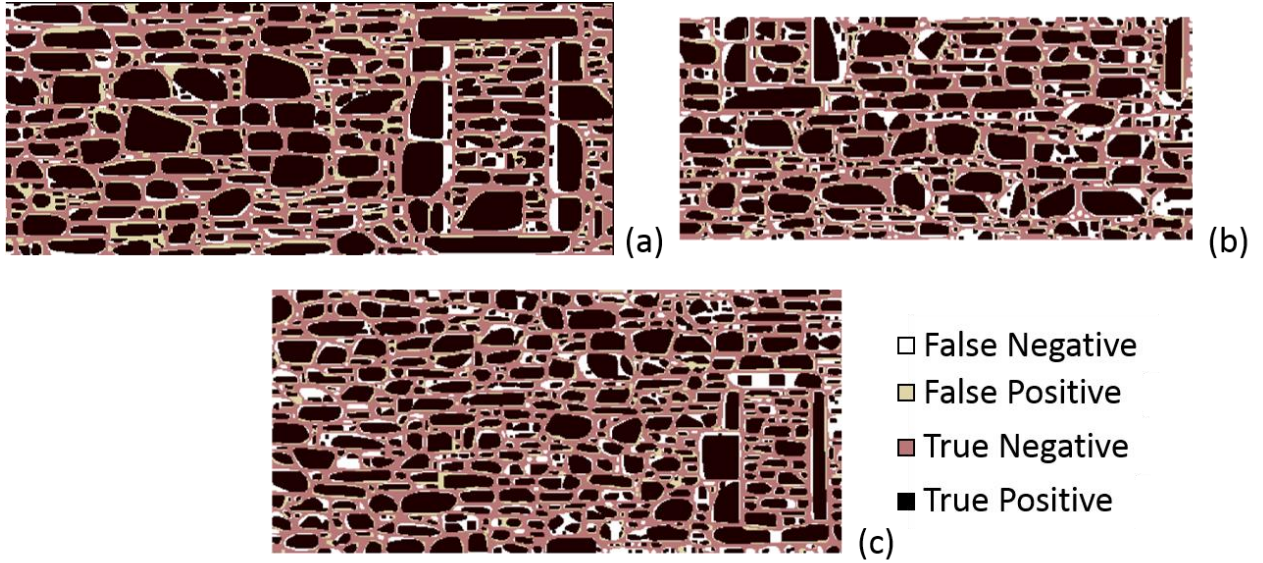
317 These factors, and their influence on the labelling of the automatically segmented stones are
 318 presented in Table 1. In this table, the 'One-to-One' column corresponds to stones in the ground truth
 319 that have been identified as a single stone by the algorithm. The other columns report the statistics
 320 for the four error cases presented above (Figure 10). As can be seen, most stones are successfully
 321 identified as one stone by the algorithm. Under-estimated stones are usually large units that, due to
 322 the irregularity of their face, are wrongly detected as several stones. Over-estimated stones are, on
 323 the contrary, small stones that, because of their close proximity, are labelled as a unique unit. Finally,
 324 missing and false stones, even if relevant in number, noticeably present small areas.

325 *Table 1: Distribution of the differences between manual and automatic segmentations*

		One-to-one	Under-estimated	Over-estimated	Missing stones	False stones
1	Number of stones	219	84	6	22	21
	Median area	53	231	85	11	15
2	Number of stones	178	67	59	36	11
	Median area	48	249	28	11	12
3	Number of stones	291	92	35	40	16
	Median area	75	204	52	14	12

326

327 Figure 11 further illustrates the segmentation performance by reporting segmentation quality at
 328 'pixel' level. In this figure 'false negatives' are regions of stone that are labelled as mortar by the
 329 algorithm, and 'false positives' are mortar regions labelled as stone.



330

331 *Figure 11: Pixel-level labelling performance results are shown for section 1 (a), section 2 (b) and section 3 (c). Black and*
 332 *yellow regions are pixels that are correctly recognized as stone (True Positive) and mortar (True Negative) respectively.*
 333 *White regions are 'false positives', i.e. mortar areas that are incorrectly labelled as stone. Yellow regions are 'false*
 334 *negatives', i.e. stone areas that are incorrectly labelled as mortar*

335

336 As can be appreciated in Figure 11, an important part of false negative areas come from the frame of
 337 blocked-up windows. These stones are architectural dressed stones. They are not rubble and impact
 338 the results mainly because of the sudden but small change in the local surface plane. Regarding false
 339 positives, these are fundamentally produced when the space between some stones is narrower than
 340 expected (i.e. areas with particularly narrow mortar joints or pinning stones close to a bigger stone).

341 From a more analytical perspective, several metrics, widely used for image segmentation evaluation,
 342 have been considered to estimate the performance of the proposed algorithms.

343 Considering the labelling of regions as True Positive (TP), True Negative (TN), False Negative (FN) and
 344 False Positive (FP), the performance of the segmentation of each stone can be given by the correctness
 345 of this labelling. Similar to the metrics presented in [32], True Positive Area Fraction (TPAF) and True
 346 Negative Area Fraction (TNAF) represent the area properly labelled. TPAF measures, for each stone,
 347 the fraction of the stone area that has been properly segmented by the algorithm. On the other hand,
 348 TNAF quantifies the area of mortar correctly identified in the surroundings of each stone. These
 349 parameters are calculated as seen in (1) and (2).

350
$$TPAF = \frac{TP}{TP+FN} \quad \text{with } TPAF \in [0,1] \quad (1)$$

351
$$TNAF = \frac{TN}{TN+FP} \quad \text{with } TNAF \in [0,1] \quad (2)$$

352 Tanimoto coefficient (Tc) [33] represents a similarity ratio between two images. In this paper, this
 353 coefficient measures the similarity of each manually segmented stone (S_A) and its corresponding
 354 segment (or segments) identified by the algorithm (S_B) as detailed in (3),

355
$$Tc = \frac{\sum_{i=1}^n S_{Ai} \cdot S_{Bi}}{\sum_{i=1}^n S_{Ai}^2 + \sum_{i=1}^n S_{Bi}^2 - \sum_{i=1}^n S_{Ai} \cdot S_{Bi}} \quad \text{with } Tc \in [0,1] \quad (3)$$

356 where n is the number of pixels of the bounding box containing S_A and S_B , and the value of S_{Ai} (and
357 S_{Bi}) is 1 if the pixel is labelled as stone, and 0 otherwise.

358 Note that T_c can also be represented by using the labelling illustrated in Figure 11 as shown in (4).

359
$$T_c = \frac{TP}{TP+FP+FN} \quad (4)$$

360 Table 2 shows the median, mean and standard deviation values of the aforementioned metrics for all
361 the stones on the evaluated wall sections. Note that, while T_c and TPAF deliver information about the
362 performance of stone segmentation, TNAF evaluates the labelling of mortar regions. The relatively
363 high values of T_c , and TPAF mean that stones areas have been segmented well. On the contrary, the
364 lower value of the coefficient TNAF implies that mortar regions have been underestimated in size in
365 some parts, mostly due to the effect of regions with narrow mortar joints (under the aforementioned
366 scale a) which are not properly segmented. This means that the algorithms classify mortar areas as
367 stone when stones are too close to one another, increasing the FP coefficient and decreasing TNAF.

368 *Table 2: Segmentation performance parameters*

	T_c	TPAF	TNAF
Median	0.68	0.83	0.60
Mean	0.63	0.77	0.58
Standard deviation	0.20	0.20	0.22

369

370 5.2. Applying the developed tool to complete 'planar' walls

371 The previous section shows the promising performance of the algorithm proposed for rubble stone
372 wall segmentation. In this section, the value of such automated segmentation is demonstrated at
373 larger scale, for complete walls. Results for the west wall of Linlithgow Palace courtyard (Figure
374 12(a)) and the rampart facing the east garden of Craigmillar Castle (

375 Figure 13(a)) are detailed in the following paragraphs.

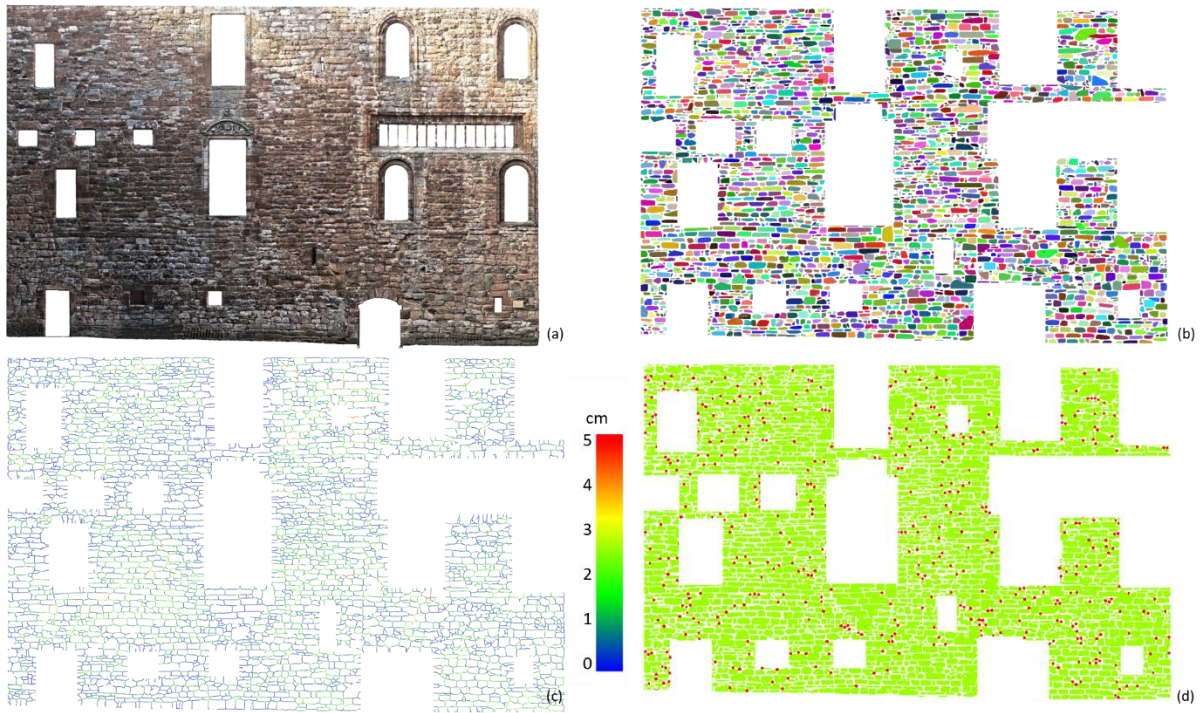
376 In both cases, different architectural components, such as windows, doors, buttresses and
377 crenellations, have been manually removed from the point cloud, as these elements are not meant to
378 be processed by means of the method proposed in this paper; they are not 'wall' components. Only
379 the points corresponding to the building component 'wall' were processed by the algorithm detailed
380 above.

381 Figure 12(b) and

382 Figure 13(b) show the stones detected in the walls, and Figure 12(c) and

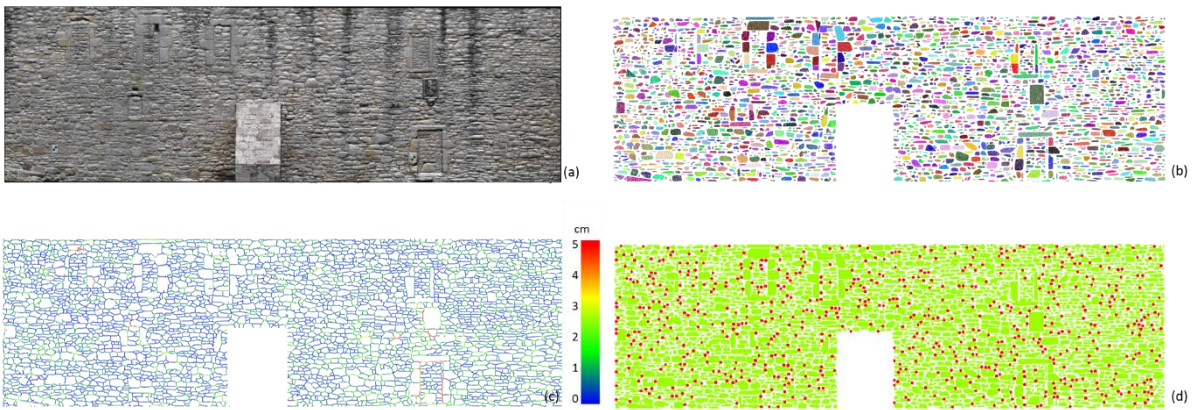
383 Figure 13(c) the mortar regions with their calculated depth. Figure 12(d) and

384 Figure 13(d) show locations where pinning may be required. Table 3 summarises information
385 automatically obtained for both walls. Even though ground truth (i.e. manual) segmentations for the
386 large datasets have not been generated, visual inspection suggests that the segmentation
387 performance is similar to that reported above for the smaller section of the Craigmillar Castle wall.



388

389 *Figure 12: Linlithgow Palace courtyard west wall. a) 3D coloured point cloud, b) Segmented and labelled stones, c) mortar*
 390 *depth map and d) Potential pinning stone locations*



391

392 *Figure 13: Craigmillar east garden rampart. a) 3D coloured point cloud, b) Segmented and labelled stones, c) mortar*
 393 *depth map and d) Potential pinning stone locations*

394 *Table 3: Quantitative parameters extracted after the automatic stone segmentation of Craigmillar and Linlithgow walls*

	Craigmillar Castle	Linlithgow Palace
Wall area	21.3 x 6.3m (= 128.42m ² without buttress area)	21.5 x 13.5m (= 196.75m ² without windows and doors)
Detected stones	2952	3056
Area covered by stone	70.74m ²	128.83m ²
Stone size (mean)	239.63 cm ²	421.56 cm ²
Linear measurement of mortar	1.18km	1.44km
Area covered by mortar	57.68m ²	67.95m ²
Depth of centre line of mortar (mean ± std)	0.92cm ± 8.2mm	1.05cm ± 8.2mm

395

396 As can be noticed in Table 3, the number of stones and the length of mortar is similar in both walls,
397 although the façade of Linlithgow Palace is twice as large as the one at Craigmillar. This suggests, and
398 this is computationally confirmed thanks to the automated segmentation, that the Linlithgow stones
399 are approximately twice as large. These results are interesting from the point of view of estimations
400 for maintenance and repair works. It shows that rules-of-thumb for estimating the amount of mortar
401 based on the wall size could easily lead to incorrect results if stone sizes are incorrectly estimated,
402 which is particularly difficult in cases where stone sizes vary significantly.

403 5.3. Applying the developed tool to curved walls

404 As presented in Section 3, the proposed approach for ‘planar’ walls can be easily applied to ‘cylindrical’
405 walls by using a point cloud unwrapping procedure (instead of a planar projection method). In this last
406 section, we show visually the working of this approach with real-life data acquired from a turret of
407 Craigmillar Castle. Figure 14 shows the original data (a; b), the unwrapped coloured data (c), the result
408 of the segmentation applied to the unwrapped data (d), and the final segmentation results re-mapped
409 onto the point cloud (e).

410 6. Conclusions

411 This paper has presented a new tool to help conservation and construction professionals better
412 understand and more objectively evaluate historic rubble masonry during survey operations. The
413 results obtained demonstrate that reasonably complete and reliable information can be attained by
414 means of a fast, cost-effective and safe survey strategies adopting these technologies.

415 Although this approach delivers added value to current surveying techniques and provides important
416 information for historic interpretation purposes, further works will be conducted to perform analysis
417 of relevant geometric and colour-related information from stones and mortar. This future research
418 encompasses the detection and identification of defects on the fabric to keep track of the records and
419 create a powerful tool for building surveying.

420 This valuable information will be stored in structured and semantic models, by integrating the
421 presented method in a holistic solution harnessing Building Information Modelling (BIM) and
422 Geographic Information Systems (GIS) technologies.

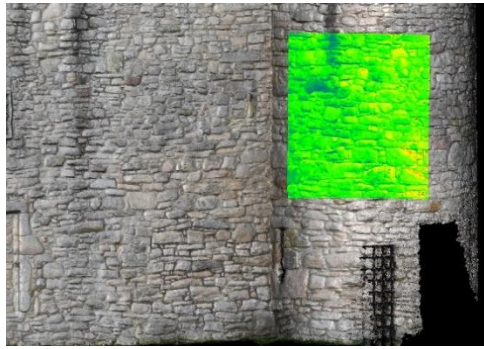
423

424 Acknowledgements

425 This paper was made possible thanks to research funding from Historic Environment Scotland. The
426 views and opinions expressed in this article are those of the authors and do not necessarily reflect the
427 official policy or position of Historic Environment Scotland. The authors would also like to acknowledge
428 the Historic Environment Scotland Digital Documentation, Science and Estates Survey team for their
429 support, in particular by providing us with the point cloud data used in the experiments reported in
430 this paper.

431

432

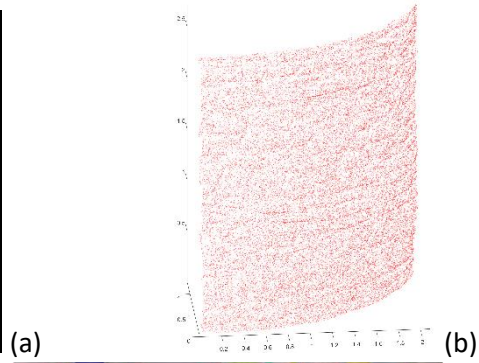


(a)

433



(c)

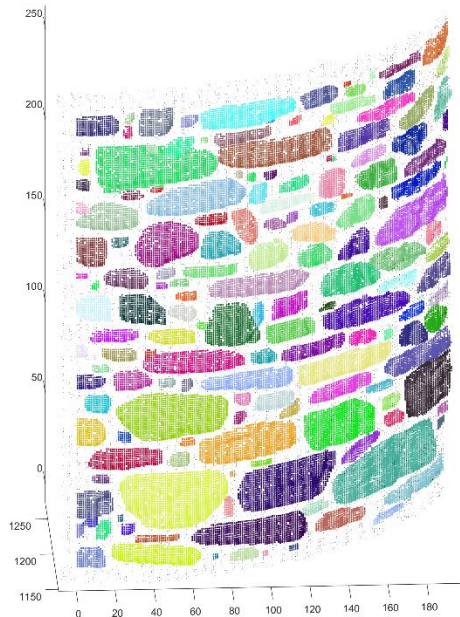


(b)



(d)

434



(e)

435 *Figure 14: Stone segmentation for surfaces for a cylindrical turret of Craigmillar Castle (Scotland). a) Region of interest, b)*
 436 *Input 3D point cloud, c) unwrapped data, d) 2D segmentation map, and e) final segmentation re-mapped onto the 3D point*
 437 *cloud.*

438

- [1] G. Mueller, J. Robertson, C. Leadbetter, N. Laing and M. a. K. A. McMenemy, "Scottish House Conditions Survey 2013. Key Findings," Scottish Government, 2014.
- [2] M. Cassar and C. Hawkings, "Engineering Historic Futures. Stakeholders Dissemination and Scientific Research Report," University College London , London, 2007.
- [3] M. Hulme, G. J. Jenkins, X. Lu, J. R. Turnpenny, M. T. D., R. G. Jones, J. Lowe, J. M. Murphy, D. Hassell, P. Boorman, R. McDonald and S. Hill, "Climate Change Scenarios for the United Kingdom: The UKCIP02 Scientific Report.," School of Environmental Sciences, University of East Anglia, Norwich, UK, 2002.
- [4] C. Hall, A. Hamilton, W. D. Hoff, H. A. Viles and J. A. Eklund, "Moisture dynamics in walls: response to micro-environment and climate change," *Proceedings of the Royal Society of London A: Mathematical, Physical and Engineering Sciences*, 2010.
<https://doi.org/10.1098/rspa.2010.0131>.
- [5] D. Young, H. C. of New South Wales, H. Victoria, S. A. D. for Environment, Heritage and A. (. Corporation, Salt Attack and Rising Damp : A Guide to Salt Damp in Historic and Older Buildings, [2nd ed.] ed., Heritage Council of NSW, Heritage Victoria, South Australian Department for Environment and Heritage, Adelaide City Council, 2008.
- [6] B. W. B. Smith and R. Magee, "Assessment of Building Stone Decay: A Geomorphological Approach," in *Proceedings of the International Conference of Stone Cleaning and the Nature, Soiling and Decay Mechanisms of Stone*, London, 1992.
- [7] A. Henry, *Stone Conservation*, Routledge, 2006.
- [8] R. Webster, *Stone Cleaning and the Nature, Soiling and Decay Mechanisms of Stone*, Donhead, London, 1992.
- [9] J. Senior, S. Semple, A. Turner and S. Turner, "Petrological Analysis of the Anglo-Saxon and Anglo-Norman Stonework of St Peter's, Wearmouth and St Paul's, Jarrow," Newcastle University, Newcastle, UK, 2014.
- [10] RICS, "Guide to Building Surveys and Inspections of Commercial and Industrial Property," 2005.
- [11] A. M. Forster and J. Douglas, "Condition Survey Objectivity and Philosophy Driven Masonry Repair: An Increased Probability for Project Divergence?," *Structural Survey*, vol. 28, no. 5, pp. 384-407, 2010. <https://doi.org/10.1108/02630801011089173>.
- [12] C. L. Ogleby, "Advances in the Digital Recording of Cultural Monuments," *ISPRS Journal of Photogrammetry and Remote Sensing*, vol. 50, no. 3, pp. 8-19, 1995.
[https://doi.org/10.1016/0924-2716\(95\)91286-S](https://doi.org/10.1016/0924-2716(95)91286-S).
- [13] L. Wilson, A. Rawlinson, D. Mitchell, H. McGregor and R. Parsons, "The Scottish Ten Project: Collaborative Heritage Documentation," in *International Archives of the Photogrammetry*,

Remote Sensing and Spatial Information Sciences, Volume XL-5/W2. XIV International CIPA Symposium, Strasbourg, 2013. <https://doi.org/10.5194/isprsarchives-XL-5-W2-685-2013>.

- [14] D. Lowe, "Object Recognition from Local Scale-Invariant Features," in *Proceedings of the International Conference on Computer Vision*, 1999. <https://doi.org/10.1109/ICCV.1999.790410>.
- [15] H. Bay, T. Tuytelaars and L. van Gool, "SURF: Speeded Up Robust Features," in *Proceedings of the European Conference on Computer Vision*, 2006. . https://doi.org/10.1007/11744023_32.
- [16] C. Strecha, T. Tuytelaars and L. Van Gool, "Dense Matching of Multiple Wide-baseline Views," in *Proceedings of International Conference on Computer Vision, ICCV 2003, Nice, France, 2003*. <https://doi.org/10.1109/ICCV.2003.1238627>.
- [17] P. Zarco-Tejada, R. Diaz-Varela, V. Angileri and P. Loudjani, "Tree Height Quantification Using Very High Resolution Imagery Acquired from an Unmanned Aerial Vehicle (UAV) and Automatic 3D Photo-Reconstruction Methods," *European Journal of Agronomy*, vol. 55, pp. 89-99, 2014. <https://doi.org/10.1016/j.eja.2014.01.004>.
- [18] P. Rodriguez-Gonzalvez, D. Gonzalez-Aguilera, G. Lopez-Jimenez and I. Picon-Cabrera, "Image-Based Modeling of Built Environment from an Unmanned Aerial System," *Automation in Construction*, vol. 48, pp. 44-52, 2014. <https://doi.org/10.1016/j.autcon.2014.08.010>.
- [19] H. Püschel, M. Sauerbier and H. Eisenbeiss, "A 3D Model of Castle Landenberg (CH) from Combined Photogrammetric Processing of Terrestrial and UAV-Based Images," in *The International Archives of the Photogrammetry, Remote Sensing and Spatial Information Sciences*, Beijing, 2008.
- [20] A. Koutsoudis, B. Vidmar, G. Ioannakis, F. Arnaoutoglou, G. Pavlidis and C. Chamzas, "Multi-Image 3D Reconstruction Data Evaluation," *Journal of Cultural Heritage*, vol. 15, pp. 73-79, 2014. <https://doi.org/10.1016/j.culher.2012.12.003>.
- [21] N. Oses and F. Dornaika, "Image-Based Delineation of Built Heritage Masonry for Automatic Classification," in *Image Analysis and Recognition*, vol. 7950, M. Kamel and A. Campilho, Eds., Springer Berlin Heidelberg, 2013, pp. 782-789. https://doi.org/10.1007/978-3-642-39094-4_90.
- [22] V. Cappellini, C. Stefani, N. Nony and L. De Luca, "Surveying Masonry Structures by Semantically Enriched 2.5D Textures: A New Approach," in *Progress in Cultural Heritage Preservation*, vol. 7616, M. Ioannides, D. Fritsch, J. Leissner, R. Davies, F. Remondino and R. Caffo, Eds., Springer Berlin Heidelberg, 2012, pp. 729-737. https://doi.org/10.1007/978-3-642-34234-9_77.
- [23] P. S. Addison, *The Illustrated Wavelet Transform Handbook: Introductory Theory and Applications in Science, Engineering, Medicine and Finance*, CRC Press, 2002.
- [24] F. Bosché and B. Biotteau, "Terrestrial laser scanning and continuous wavelet transform for controlling surface flatness in construction – A first investigation," *Advanced Engineering Informatics*, vol. 29, no. 3, pp. 591-601, 2015. <https://doi.org/10.1016/j.aei.2015.05.002>.

- [25] E. Valero and F. Bosché, "Automatic Surface Flatness Control using Terrestrial Laser Scanning Data and the 2D Continuous Wavelet Transform," in *Proceedings of the 33rd ISARC*, Auburn (USA), 2016. <https://doi.org/10.22260/ISARC2016/0007>.
- [26] M. Fischler and R. Bolles, "Random sample consensus: a paradigm for model fitting with applications to image analysis and automated cartography," *Communications of the ACM*, vol. 24, no. 6, pp. 381-395, 1981. <https://doi.org/10.1145/358669.358692>.
- [27] P. H. S. Torr and A. Zisserman, "MLESAC: A New Robust Estimator with Application to Estimating Image Geometry," *Computer Vision and Image Understanding*, vol. 78, no. 1, pp. 138-156, 2000. <https://doi.org/10.1006/cviu.1999.0832>.
- [28] T. M. Apostol and M. A. Mnatsakanian, "Unwrapping Curves from Cylinders and Cones," *The American Mathematical Monthly*, vol. 114, pp. 388-416, 2007.
- [29] BSI, "BS 5628-3:2005. Code of practice for the use of masonry. Materials and components, design and workmanship," BSI, 2005.
- [30] P. Gibbons, "TAN 1: Preparation and Use of Lime Mortars," Historic Environment Scotland, Edinburgh, 2003.
- [31] T.-C. Lee, R. L. Kashyap and C.-N. Chu, "Building Skeleton Models via 3D Medial Surface/Axis Thinning Algorithms," *Computer Vision, Graphics and Image Processing*, vol. 56, no. 6, pp. 462-478, 1994. <https://doi.org/10.1006/cgip.1994.1042>.
- [32] J. K. Udupa, V. R. LeBlanc, Y. Zhuge, C. Imielinska, H. Schmidt, L. M. Currie, B. E. Hirsch and J. Woodburn, "A framework for evaluating image segmentation algorithms," *Computerized Medical Imaging and Graphics*, vol. 30, no. 2, pp. 75-87, 2006. <https://doi.org/10.1016/j.compmedimag.2005.12.001>.
- [33] T. Tanimoto, "An Elementary Mathematical theory of Classification and Prediction," International Business Machines Corporation, 1957.

441

442